Computational evaluation of new lithium-3 garnets for lithium-ion battery applications as anodes, cathodes, and solid-state electrolytes

Muratahan Aykol, Soo Kim, Vinay I. Hegde, Scott Kirklin, and Chris Wolverton

Computational Evaluation of New Lithium-3 Garnets for Lithium-ion Battery Applications as Anodes, Cathodes, and Solid-State Electrolytes

Muratahan Aykol,[a,1] Soo Kim,[a,2] Vinay I. Hegde,[a] Scott Kirklin,[a] and Chris Wolverton[a,]*

[a] Department of Materials Science and Engineering, 2220 Campus Drive, Evanston IL, USA

[1] Present Address: Toyota Research Institute, Los Altos CA, USA

[2] Present Address: Robert Bosch Research and Technology Center, Cambridge MA, USA

*Correspondence: c-wolverton@northwestern.edu

Abstract

In this work, we explore a set of new garnet oxide structures that can be used as an anode, cathode or solid-electrolyte in lithium-ion batteries (LIBs) using high-throughput density functional theory. We test around 180 combinations of elemental substitutions for the dodecahedral X sites and octahedral Y sites in the $Li_3X_3Y_2O_{12}$ type garnet structure and identify 19 stable (*i.e.*, on the convex-hull) and 11 nearly stable (*i.e.*, within 50 meV/atom of the convex-hull) Li_3-garnets with respect to decomposition to other stable phases in the Open Quantum Materials Database (OQMD) in the respective 4-dimensional Li-X-Y-O chemical spaces. Our high-throughput screening strategy allows us to elucidate rules for garnet stability in terms of the ionic radii of the constituent elements. We evaluate the electrochemical window (EW) of these new, stable/nearly stable Li_3-garnet compounds and classify each for potential applications as an anode, cathode, or solid-state electrolyte to be used in LIBs. Finally, Li^+ ion diffusivity is calculated for the representative $Li_3Nd_3W_2O_{12}$ model system. Results we present here are expected to serve as a guideline for designing new garnet oxides for Li-ion battery applications.

I. Introduction

Research and development of high-performance energy storage technologies that are more cost-effective and cleaner has been of significant interest for applications ranging from portable electronic devices to emerging electric vehicles. Specifically, there has been a recent, collective research effort to explore all-solid-state battery systems as a possible new class of energy storage systems, beyond conventional lithium-ion batteries (LIBs) [1-4]. In such all-solid-state systems, fast ion conducting ceramics play a key role as the solid-state-electrolyte (SSE), as they would replace the flammable organic electrolytes, and potentially enable the use of Li-metal as an anode component. Among many candidates, lithium garnets have been suggested as a promising class of materials that can serve multiple roles, from anode to cathode to electrolyte, to achieve all-solid-state Li-ion batteries [3,5-7]. As a battery component, the garnet structure can accommodate a significant amount of lithium [6]; and, (*de-*)insertion of lithium ions is often possible when a redox active transition metal is present within the garnet host structure. Moreover, the relatively open crystal structure of certain garnets may allow fast Li^+ ion conduction. For example, the overlithiated garnet $Li_7La_3Zr_2O_{12}$ (LLZO) has been investigated extensively for SSE applications [6,8,9]. Recently, Goodenough and his co-workers have introduced the $Li_3Nd_3W_2O_{12}$ garnet oxide as a high-power anode material for LIBs [10,11]. Such lithium garnets have the formula of $Li_3X_3Y_2O_{12}$, where the chemical identity of the elements occupying X and Y sites control the resulting structural, thermodynamic, electrochemical, and ionic-transport properties of the material.

Well-known examples of garnets are naturally occurring silicate minerals $X_3Y_2(SiO_4)_3$ [12]. In this mineral, the X sites are often occupied by the divalent Ca^{2+}, Mg^{2+}, and Fe^{2+} ions, and Y sites are often occupied by the trivalent Al^{3+}, Fe^{3+}, and Cr^{3+} ions [13]. Similarly, lithium

2

garnets have the general formula $Li_3X_3Y_2O_{12}$, where Li replaces Si and resides in the tetrahedral sites, and thus X and Y typically need to be occupied by higher valence ions compared to the natural minerals. The $Li_3X_3Y_2O_{12}$ garnet has a cubic structure with the *Ia$\bar{3}$d* space group, and is illustrated in **Figure 1**. The X sites (24*c*) are 8-fold (dodecahedral), Y sites (16*a*) are 6-fold (octahedral), and Li (24*d*) sites are 4-fold (tetrahedral) oxygen anion (O^{2-}) coordinated, respectively. Oxygen atoms occupy the 96*h* sites. Due to the dodecahedral coordination, X sites are usually occupied by larger (or, lower valence) cations, compared to Y sites. Most of the transition metal ions can easily fit into the Y sites. It is possible to further (*de-*)lithiate $Li_3X_3Y_2O_{12}$ by Li insertion or extraction, as long as a redox-active cation is present in X and/or Y sites, as in $Li_3Nd_3W_2O_{12}$. The 3-D channels in the relatively open structure where Li ions can transport relatively fast, and the robust crystal structure make Li_3-garnets a promising class of materials for solid-state battery applications, from electrodes to electrolytes.
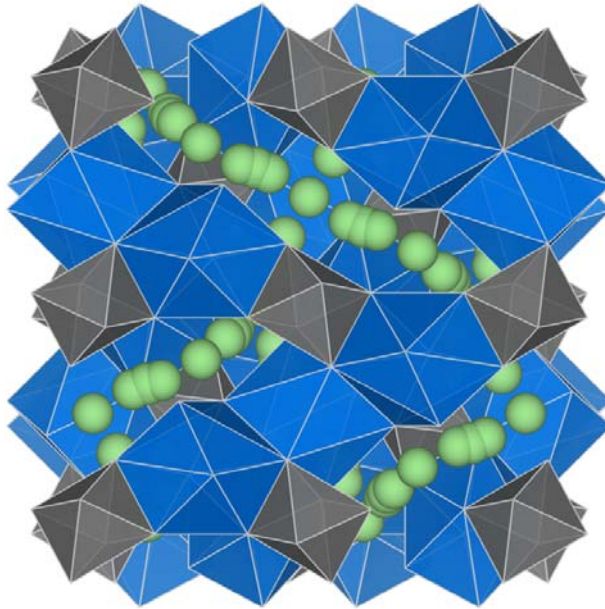
Figure 1. Schematics of the $Li_3X_3Y_2O_{12}$ garnet structure. Dodecahedral (blue) and octahedral (gray) polyhedra show X and Y sites respectively. Li sites including the 48*g* transition sites

3

are shown as spheres. O atoms occupy the corners of the polyhedra and are not visible in the figure for clarity.

To date, there have been several densify functional theory (DFT)-based theoretical studies in order to help understand the materials properties of these lithium-containing ceramic superionic conductors [2-4,14-22]. Also, high-throughput DFT (HT-DFT) screening strategies have been employed to screen and design new battery materials such as anodes [23], cathodes [24-26], electrolytes [4], and coatings [27,28]. In this work, using the Open Quantum Materials Database (OQMD) infrastructure [29,30], we perform a HT-DFT based search to explore a wide range of chemistries for the $Li_3X_3Y_2O_{12}$ garnet family by informed substitution (*e.g.*, on the basis of radii and accessible oxidation states) of various elements for X and Y sites, and report their stabilities, and electrochemical activity windows. Finally, Li-ion diffusivity is calculated for $Li_3Nd_3W_2O_{12}$ model system.

II. Computational Methods

All first-principles calculations were carried out using the Vienna Ab-initio Simulation Package (VASP) [31-33] within the OQMD framework [29,30]. We use the Perdew Burke Ernezerhof formulation of the generalized gradient approximation with the VASP-recommended set of projector augmented wave potentials. Calculations were spin-polarized when there is a d-block or actinide element in the material. A Hubbard-U was applied to elements V, Cr, Mn, Fe, Co, Ni and Cu when they exist in an oxygen bearing material, with respective U values of 3.1, 3.5, 3.8, 4.0, 3.3, 6.4 and 4.0 eV. We use a k-point grid with a density of 6,000 k-points per reciprocal atom. Further details of the DFT settings can be found in our previous studies [27-30]. Voltage and stability evaluations were performed using the OQMD database v1.1 available for public access at http://oqmd.org/download. The python scripts used to calculate stability and voltage data employing the qmpy python

package and this database are available at https://doi.org/10.5281/zenodo.1469161 along with instructions for how to access the input files (except the proprietary VASP pseudopotentials). While the data is available in the database for programmatic access, compounds generated in this work can also be accessed directly http://oqmd.org/materials/keyword/garnet.

Molecular dynamics (MD) calculations were done using the 160-atom conventional garnet cell in the NVT ensemble at the ground state volume found by DFT relaxation of the structure. A time-step of 2 femtoseconds was used in MD runs, and each MD run at a given temperature consisted of an initial equilibration period of at least 0.1 ns, and a subsequent data collection period of at least 0.2 ns. All ab-initio MD calculations were non-spin polarized, and performed with the Γ-point only at a cut-off energy of 400 eV to reduce the computational cost. For the gaseous reference state of O_2, we additionally considered the tabulated standard room temperature entropy available from the JANAF tables [34]. Visual in Figure 1 is generated using VESTA [35]. Ionic radii used in filtering were taken from Shannon [36].

Table 1. Ionic configurations for different X^{x+} and Y^{y+} pairs in $Li_3X_3Y_2O_{12}$ garnets determined on the basis of charge-balance and geometric constraints. First column lists possible combinations of oxidation states for X and Y. Second and third columns list possible X and Y elements, respectively, that can access the given oxidation states, and satisfy the radius criteria described in the text. For cases where charge-balance required non-integral nominal oxidation states for an element, we picked such elements among those that can accordingly access multiple oxidation states and yield the given non-integral oxidation state. We do not consider radioactive elements.

X^{x+} and Y^{y+}	X	Y
X^{2+}, $Y^{7.5+}$	Unlikely due to inaccessible oxidation state of 7.5+	
X^{3+}, Y^{6+}	La, Bi, Ce, Nd, Sm, Gd, Y, Yb, In, Sb, Sc, Nb, Ta, Mo, Ti, Fe, V, Ga, Cr	W, Mo, Cr, Te, Se
X^{4+}, $Y^{4.5+}$	Te, Ce, Pb, Zr, Hf	Nb, Ta, W, Mo, V, Cr

X^{5+}, Y^{3+}	Bi, Nb, Ta, W, Mo	Al, In, Ga, Y, Sc, Ti, V, Cr, Fe, Mn, Co, Cu
X^{6+}, $Y^{1.5+}$	Unlikely due to very small X^{6+} for the dodecahedral site	

Table 2. List of stable and metastable Li_3-garnets identified in this work. Garnets that are on the convex-hull are labeled as stable, and those above but within 50 meV/atom of the convex-hull are labeled as metastable. Oxygen chemical potential used in calculation of stabilities corresponds to $T = 298$ K and $p = 1$ atm.

Stability	Compounds
Stable	$Li_3Bi_3Te_2O_{12}$, $Li_3Ce_3Mo_2O_{12}$, $Li_3Ce_3Se_2O_{12}$, $Li_3Ce_3Te_2O_{12}$, $Li_3Ce_3W_2O_{12}$, $Li_3Gd3Se_2O_{12}$, $Li_3Gd_3Te_2O_{12}$, $Li_3La_3Se_2O_{12}$, $Li_3La_3Te_2O_{12}$, $Li_3La_3W_2O_{12}$, $Li_3Nd_3Se_2O_{12}$, $Li_3Nd_3Te_2O_{12}$, $Li_3Nd_3W_2O_{12}$, $Li_3Sm_3Se_2O_{12}$, $Li_3Sm_3Te_2O_{12}$, $Li_3Sm_3W_2O_{12}$, $Li_3Y_3Se_2O_{12}$, $Li_3Y_3Te_2O_{12}$, $Li_3Yb_3Te_2O_{12}$
Metastable	$Li_3Gd_3W_2O_{12}$, $Li_3La_3Mo_2O_{12}$, $Li_3Bi_3Se_2O_{12}$, $Li_3Nd_3Mo_2O_{12}$, $Li_3Y_3W_2O_{12}$, $Li_3Yb_3W_2O_{12}$, $Li_3Bi_3Co_2O_{12}$, $Li_3Sm_3Mo_2O_{12}$, $Li_3In_3Te_2O_{12}$, $Li_3Bi_3W_2O_{12}$, $Li_3Sc_3Te_2O_{12}$

III. Results and discussion

III.1. Generation of Li₃-garnet structures

OQMD framework considers 89 elements with available VASP potentials, which gives ~7,800 possible X and Y permutations in the garnet host lattice structure. However, the primitive cell of $Li_3X_3Y_2O_{12}$ has 80 atoms; and therefore is computationally expensive to relax with DFT. Thus, initially, we narrow down the list of hypothetical structures derived from the garnet-prototype to calculate. If the oxidation states of X and Y are *x* and *y*

6

respectively, the charge balance constraint for $Li_3X_3Y_2O_{12}$ can be written as $3x + 2y = 21$. It is also reasonable to expect the 8-fold coordinated X site to be occupied by relatively larger ions compared to the 6-fold coordinated Y sites. Based on Pauling's cation to anion radius ratio for transitioning from a 6-fold to 8-fold coordination (~0.732), we can roughly estimate that cations with a radius of $r > \sim 0.9$ Å are more likely to occupy the X sites (coordinated with O^{2-} with a radius of 1.26 Å). Nonetheless, the radius ratio cannot be as strict a constraint as the charge balance. Therefore, we relax this criterion and consider an element for site X if its ionic radius is larger than ~0.65 Å. This charge-balance and geometry analysis reduces the number of Li_3-garnets to calculate from ~7800 to 185. The respective X and Y pairs are listed in **Table 1**, which in turn yield 182 unique garnets, and out of these, ~95% of DFT calculations successfully converged. The complete list of Li_3-garnets calculated are available in Supplemental Material.[37]

III.2. Thermodynamic stabilities of Li₃-garnets

The stability of a compound with respect to other phases (*e.g.*, those in the OQMD [29,30]) is a critical factor to determine whether that compound can be synthesized/stabilized experimentally. Here we measure the stability as the distance of the garnet to the convex-hull (*i.e.*, lowest energy linear combination of phases at the given composition). The convex-hull evaluation includes all phases in the OQMD, including the garnets tested here. A zero distance to convex-hull means the corresponding garnet is predicted to be the ground state at its composition. Positive distances mean the garnet is above the hull, *i.e.*, can be metastable or unstable. Among the hypothetical garnets tested based on the list in Table 1, we found that only 19 of them are on the convex-hull (*i.e.*, stable) in their 4D Li-X-Y-O chemical spaces with respect to decomposition to other stable phases. In addition, there are 11 compounds within 50 meV/atom of the hull-energy, which are also included in the further analysis as

nearly-stable (*i.e.*, potentially metastable) candidates. These stable and metastable Li_3 garnets are listed in **Table 2**. Li_3-garnets previously reported as synthesized in literature [38]; namely, $Li_3Nd_3W_2O_{12}$, $Li_3Nd_3Te_2O_{12}$, $Li_3Gd_3Te_2O_{12}$ and $Li_3Y_3Te_2O_{12}$ are all captured as stable materials in our framework, validating our selection strategy. Likelihoods of laboratory synthesis of other stable Li_3-garnets found in this work (Table 2) are estimated to be ≥90%

using the recent network-based approach, with the only exception of $Li_3La_3W_2O_{12}$, which has a slightly lower likelihood of ~70%.[39]

In **Figure 2**, we show the stabilities (distance to convex-hull) of tested prototype-derived garnets as a function of ionic radii ratios among X^{x+}, Y^{y+}, and O^{2-}. We observe that $Li_3X_3Y_2O_{12}$ garnet compounds tend to be stable (*i.e.*, on the convex- hull) when the following criteria are satisfied: *i*) $r_{X^{x+}}/r_{O^{2-}} > \sim 0.75$, *ii*) $r_{Y^{y+}}/r_{O^{2-}} < \sim 0.62$, and *iii*) $0.4 < r_{Y^{y+}}/r_{X^{x+}} < 0.8$. Therefore, the $r_{X^{x+}}/r_{O^{2-}}$ of stable garnets is clearly in line with the ideal 6 to 8-fold coordination transition at the ratio of 0.732. The $r_{Y^{y+}}/r_{O^{2-}}$ of stable candidates also indicate that occupation of Y site by atoms with smaller radii favor stability. Based on $r_{Y^{y+}}/r_{X^{x+}}$, we clearly see that ion Y has to be a much smaller cation than X to ensure stability.

The decomposition products of the metastable garnets are listed in **Table 3** along with their distance from the ground-state convex-hull. Only three compounds are found to be within 25 meV/atom of the hull. The larger the distance to the convex-hull is, the higher will be the driving force for the metastable garnet to decompose into the listed phases. In addition, the compounds that release oxygen upon decomposition, such as $Li_3Bi_3Se_2O_{12}$, $Li_3Bi_3Co_2O_{12}$, and $Li_3Yb_3Se_2O_{12}$ should be considered carefully in battery applications as oxygen release might be a critical safety hazard.
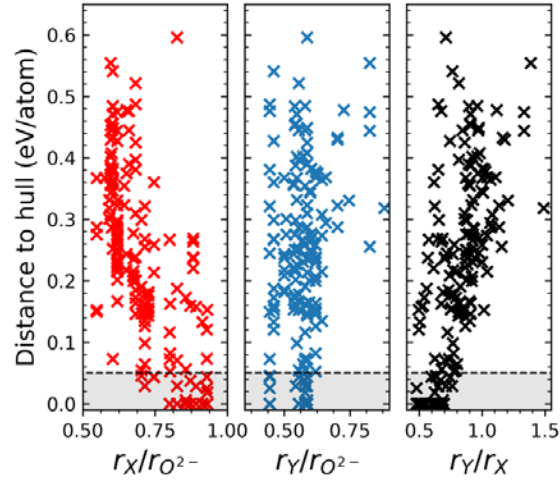
Figure 2. Thermodynamic stabilities of Li_3-garnets against decomposition into more stable phases on the convex-hull as functions of ratios of ionic radii of X^{x+}, Y^{y+} and O^{2-}. Stability is measured as energetic distance to the hull (see text). Oxygen chemical potential corresponds to 1 atm and $T = 298$ K. Shaded areas show the stability range considered up to 2 kT 50 meV/atom. For cases where an exact oxidation state − radius match could not be found, we use the closest matching radius in *Ref.* [36].

Table 3. Decomposition products and their energies relative to the convex-hull for the nearly stable (*i.e.*, metastable) Li_3-garnets. ΔE denotes the distance to hull measured in meV/atom. Oxygen chemical potential corresponds to $T = 298$ K and $p = 1$ atm.

Compound	Convex-hull Composition	ΔE	Note
$Li_3Gd_3W_2O_{12}$	$3/2\ Li_2WO_4 + 1/2\ Gd_2WO_6 + Gd_2O_3$	1	-
$Li_3La_3Mo_2O_{12}$	$1/2\ La_2MoO_6 + La_2O_3 + 3/2\ Li_2MoO_4$	17	-
$Li_3Y_3W_2O_{12}$	$1/2\ Y_6WO_{12} + 3/2\ Li_2WO_4$	24	-
$Li_3Yb_3Se_2O_{12}$	$3\ YbO + 3/2\ Li_2SeO_4 + 1/2\ SeO_2 + O_2$	26	O_2 release
$Li_3Nd_3Mo_2O_{12}$	$Nd_2O_3 + 3/2\ Li_2MoO_4 + 1/2\ Nd_2MoO_6$	27	-
$Li_3Sm_3Mo_2O_{12}$	$Sm_2O_3 + 3/2\ Li_2MoO_4 + 1/2\ Sm_2MoO_6$	32	-
$Li_3Bi_3Co_2O_{12}$	$2/3\ Co_3O_4 + 3\ LiBiO_3 + 1/6\ O_2$	38	O_2 release
$Li_3Bi_3W_2O_{12}$	$3/2\ Li_2WO_4 + 1/2\ Bi_2WO_6 + Bi_2O_3$	39	-
$Li_3Bi_3Se_2O_{12}$	$1/8\ Bi_4O_7 + 5/4\ Bi_2SeO_5 + 3\ Li_4SeO_5 + 9/16\ O_2$	40	O_2 release
$Li_3In_3Te_2O_{12}$	$5/4\ In_2TeO_6 + 1/4\ In_2O_3 + 3/4\ Li_4TeO_5$	42	-
$Li_3Sc_3Te_2O_{12}$	$1/4\ Sc_2O_3 + 5/4\ Sc_2TeO_6 + 3/4\ Li_4TeO_5$	46	-

III.3. Electrochemical windows of Li₃-garnets

The stability range of the material upon reduction and oxidation, *i.e.*, electrochemical

window (EW), is one of the most fundamental properties for battery materials. EW determines whether the material is suitable electrolyte applications, or worth further exploring as a certain type of electrode (anode or cathode). For all stable and metastable Li_3-garnets predicted, we calculate the EWs as shown in **Figure 3.** To measure the electrochemical stability, we consider two different approaches: *i*) dilute limit lithium (*de-*)insertion potentials and *ii*) bulk potentials calculated from the Li-X-Y-O convex-hull. In approach *i*), we (*de-*)insert one Li atom into (or *from*) the garnet structure. For Li insertion, *i.e.*, reduction of the garnet, we put one Li atom on one of the symmetrically equivalent octahedral 48*g* sites of the 80-atom garnet supercell. The inserted Li atom can also be displaced to the 96*h* positions near the facets of the empty tetrahedral sites [10]; and, therefore we also test that Li configuration, accordingly. For Li extraction, we remove one of the 12 existing, symmetrically equivalent Li atoms occupying the 24*d* sites. This procedure yields the "dilute-limit" insertion/extraction window of the garnet, and is important upon classifying it as an anode, a cathode, or an electrolyte. However, the absolute stability of the garnet upon oxidation or reduction is dictated by the phases that are on the convex-hull. Thus, in approach *ii*), we also calculate the "ground-state" stability windows, from the actual OQMD convex-hull of the Li-X-Y-O. We calculate these windows in a way similar to the lithiation voltages of generic coatings described in our previous studies [27,28], and therefore we do not repeat the methodology here (See Supplemental Materials [37]). It is important to note that for all stable garnets, this "bulk" electrochemical window is narrower than the dilute-limit (insertion) one in **Figure 3**, meaning the mixture of bulk phases on the OQMD convex-hull are always more stable than the Li-inserted/extracted garnet structures. Full bulk lithiation profiles of stable Li_3-garnets obtained from OQMD convex-hulls are available in the Supplemental Materials.[37]
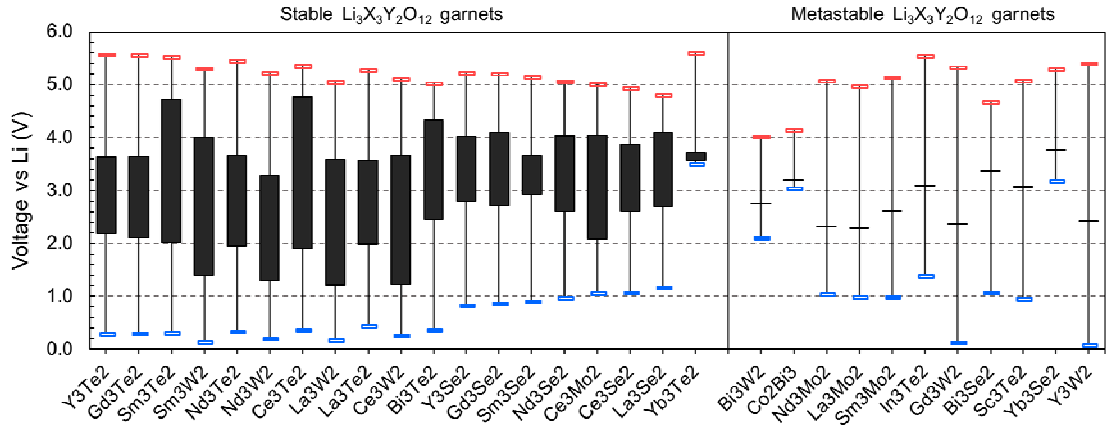
Figure 3. Electrochemical stability windows of 19 stable and 11 metastable $Li_3X_3Y_2O_{12}$ garnets calculated in this work. The wider windows correspond to the dilute limit Li-insertion and Li-extraction potentials within the garnet lattice, whereas the narrower (black-filled) windows correspond to reduction and oxidation potentials found from the OQMD[29,30] convex-hull. For metastable materials (those above the convex-hull), the latter potential does not exist by definition, and therefore for those, the average potential found at the given composition on the hull is shown as a black horizontal line. We particularly suggest the use of predicted $Li_3X_3Y_2O_{12}$ garnets as the following on the basis of the criteria described in the text: *i*) anodes: Sm_3W_2, Nd_3W_2, La_3W_2, Ce_3W_2 and Gd_3W_2; ii) cathodes: Yb_3Se_2, Yb_3Te_2, Bi_3Co_2, and Bi_3W_2; and *iii*) electrolytes: Y_3Te_2, Gd_3Te_2, Sm_3Te_2, Sm_3W_2, Nd_3Te_2, Ce_3Te_2, and La_3W_2.

For anode applications, the insertion potential of the garnet should be low. In this case, the Li_3-garnets would be the starting point of lithiation, *i.e.*, "de-insertion" is not viable as an anode as oxidation happens at significantly high potentials for all garnets studied, as is evident from the wide EWs reaching above 4-5 V vs Li. In addition, the size of the gap between the dilute-limit Li insertion (*i.e.*, reduction) potential, and the bulk reduction potential obtained from the OQMD can be considered as an indicator for the driving force for the garnet framework to convert to other thermodynamically stable compounds upon lithiation. This conversion could be kinetically sluggish compared to insertion/extraction of Li, and in fact cause the degradation of the garnet crystal structure during operation.

11

Therefore, the voltage gap described above should be as narrow as possible. To highlight these features for electrode selection, in **Figure 4,** we plot the "dilute limit" insertion potential vs. its deviation from the corresponding bulk reduction potential for all stable and metastable garnets reported in **Figure 3**. As highlighted in in **Figure 4** based on the guidelines above, we recommend four Li_3-garnets as promising for anode applications; namely, $Li_3Sm_3W_2O_{12}$, $Li_3Nd_3W_2O_{12}$, $Li_3La_3W_2O_{12}$, $Li_3Ce_2W_2O_{12}$ and $Li_3Gd_3W_2O_{12}$. Capturing the already known $Li_3Nd_3W_2O_{12}$ anode [11] within this framework validates the guidelines; and, implies that the other three garnets we predict as promising anodes are all viable candidates.

In filtering materials reported in **Figure 3** for cathode applications, we follow a similar approach as defined above for the anodes, but simply prefer the insertion voltages to be high (at least 2 V), while keeping a narrow gap between dilute and bulk window potentials to minimize the tendency to decompose upon Li-insertion, as demonstrated in **Figure 4**. We identify four garnets that would make promising cathodes; namely, $Li_3Yb_3Se_2O_{12}$, $Li_3Yb_3Te_2O_{12}$, $Li_3Bi_3Co_2O_{12}$, and $Li_3Bi_3W_2O_{12}$. None of these materials have previously been synthesized or tested, to the best of our knowledge. The EWs for these materials are not only at higher potentials but are also narrow (*i.e.*, reduction and oxidation potentials are close), implying they may also allow de-insertion of some of the existing Li in the Li_3-garnet framework when used as a cathode.

For electrolyte applications, the EWs (both the dilute-limit EWs and bulk EWs) need to be as wide as possible. Again, we prefer the gap between dilute-limit potentials and bulk potentials to be as small as possible to have a lower tendency for the electrolyte to react and precipitate other phases at the anode and cathode interfaces. We observe in **Figure 3** that many Li_3-garnets provide quite wide dilute-limit EWs, some as wide as ~5.5 V, with

reduction potentials between 0 and 1 V, and oxidation potentials between 5 and 6 V. These promising electrolyte candidates include $Li_3Y_3Te_2O_{12}$, $Li_3Gd_3Te_2O_{12}$, $Li_3Sm_3Te_2O_{12}$, $Li_3Sm_3W_2O_{12}$, $Li_3Nd_3Te_2O_{12}$, $Li_3Ce_3Te_2O_{12}$, and $Li_3La_3W_2O_{12}$, given in the order of the size of their dilute-limit (insertion/de-insertion) EWs. These electrolyte candidates also have relatively wide band gaps (all within a range of 3.4 – 3.6 V as calculated with DFT, therefore likely to be even wider in experiments), which is desirable for electrolyte applications. Among the candidates listed, $Li_3Sm_3W_2O_{12}$, $Li_3Nd_3Te_2O_{12}$, and $Li_3Ce_3Te_2O_{12}$ exhibit relatively larger bulk EWs, and therefore are likely to be thermodynamically more stable as solid electrolytes.
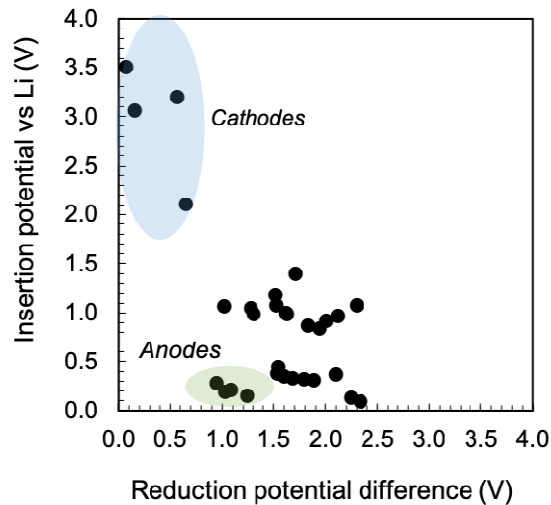
Figure 4. Identifying the promising anode and cathode candidates among Li_3 garnets: insertion potentials (vertical axis) plotted against their deviation from the corresponding *bulk* reduction potentials calculated from the OQMD convex-hulls (horizontal axis). Ideal anode and cathode materials would lie towards the lower and upper left corners of the plot, respectively, and promising materials that demonstrate the closest potentials to these ideal limits are highlighted accordingly.

III.4. Lithium-ion diffusivity in Li₃-garnets

Lithium-ion diffusivity of the garnet lattice is critical for all battery applications above. To evaluate that, we have selected $Li_3Nd_3W_2O_{12}$ as a model system to represent all other similar Li_3-garnets in **Figure 3** and carried out *ab*-initio molecular dynamics (MD) calculations to extract Li-ion diffusivities. The Li-ion diffusion coefficients, D_{Li}, are obtained from the variation of mean-squared-displacement with time (t), as in the well-known relation: $D = \frac{1}{6}\lim_{t\to\infty}\langle|\mathbf{r}(t) - \mathbf{r}(0)|^2\rangle$. Here $\mathbf{r}(t)$ denotes the atomic positions at t. D_{Li} obtained from the MD runs at various temperatures are shown in **Figure 5**. We find that the activation barrier Q for Li diffusion is 0.71 eV for $Li_{24+1}Nd_{24}W_{16}O_{96}$, and the estimated room temperature D_{Li} is around 6×10^{-15} cm^2/s. While this coefficient is a few orders of magnitude smaller than the typical electrolytes utilized in Li-ion batteries, it is still at a reasonable level for an electrode material [40]. Thus, we conclude that Li-diffusivities need to be enhanced in these Li_3-garnet oxides, especially for electrolyte applications. This can be achieved experimentally by introducing defects, doping, or, as well-known for the stuffed (Li-rich) garnet-type Li-ion conductors (*e.g.*, LLZO), by increasing Li-content [3,6,14,41]. In Li_3-garnets, Li occupies only the tetrahedral sites, whereas in garnets with higher Li contents, Li starts occupying the intermediate octahedral sites and Li-vacancies are created on the tetrahedral sites, overall, resulting in enhanced lithium-ion diffusivity [6,38]. To validate this hypothesis for the present Li_3 garnets, we calculated the activation barrier, Q as a function of Li content in other $Li_{3+x}Nd_3W_2O_{12}$ compositions using ab-initio MD as shown in **Figure 6**. A significant drop in Q to levels comparable to LLZO and similar fast-ion conductors is found at about x ~ 0.25 – 0.5 in $Li_{3+x}Nd_3W_2O_{12}$. The estimated room temperature D_{Li} values at these compositions are around 10^{-9} cm^2/s, close to typical commercial electrodes and other ion-conducting garnets [38,40]. While future work is required to fully evaluate lithium-ion diffusivity for other predicted Li_3-garnet structures, given their chemical similarity to Nd_3W_2, we expect the

present trends in diffusion to reasonably extend to such systems including Ce_3Te_2, La_3W_2, Nd_3Te_2, Sm_3Te_2, and Sm_3W_2.
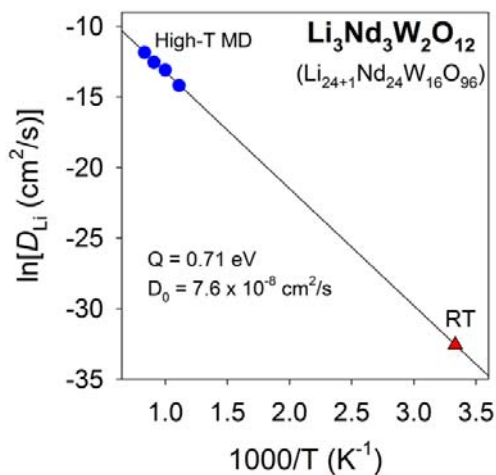
Figure 5. Lithium-ion diffusivities D_{Li}, obtained at various temperatures with ab-initio MD runs (circles), along with the calculated activation barrier and D_0 assuming an Arrhenius-type relation of $D = D_0 exp\left(-\frac{}{}\right)$. The room temperature value estimated based on this relation is also shown (triangle).
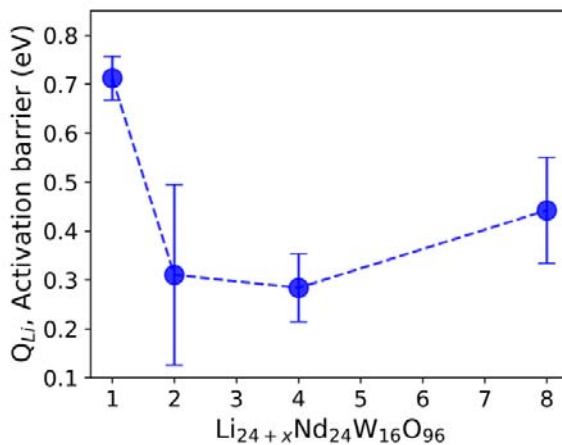
Figure 6. Activation barrier, Q, for the lithium ion diffusion in $Li_{3+x}Nd_3W_2O_{12}$ as a function of additional lithium content, x as obtained from high-temperature ab-initio MD simulations. Error bars show the standard deviation in the slope (Q) in linear regression for lnD vs $1/T$ (See Supplemental Materials [37]).

IV. Conclusion

We have evaluated the thermodynamic stabilities, electrochemical windows, and diffusivities of Li_3-type garnets analogous to $Li_3Nd_3W_2O_{12}$ by utilizing the high-throughput density functional theory-based infrastructure of the OQMD. Among a list of ~180 $Li_3X_3Y_2O_{12}$ type garnets selected based on geometric and charge-balance arguments for X and Y, only 19 X_3Y_2 combinations are found to be thermodynamically stable against decomposition into other phases in the OQMD, and 11 combinations are metastable within 50 meV/atom of the convex-hull. In these (meta)-stable phases, in analogy with $Li_3Nd_3W_2O_{12}$, X is often found to be a rare-earth metal, and Y is one of Te, Se, W, and Mo. By comparing the dilute-limit lithium insertion and extraction potentials to that obtained from the bulk OQMD phase diagrams, we were able to classify these Li_3-garnets as promising anodes, cathodes, and electrolytes. While we found viable candidates for each category, Li-diffusion calculations for the model $Li_3Nd_3W_2O_{12}$ system indicate that ionic conductivity of such Li_3-garnet materials may need to be enhanced prior to practical applications, especially as a solid-state electrolyte for LIBs and small increases in Li content are found to promote Li diffusivity.

References

[1] N. Kamaya, K. Homma, Y. Yamakawa, M. Hirayama, R. Kanno, M. Yonemura, T. Kamiyama, Y. Kato, S. Hama, K. Kawamoto, and A. Mitsui, *Nat. Mater.* **10**, 682 (2011).

[2] Y. Mo, S. P. Ong, and G. Ceder, *Chem. Mater.* **24**, 15 (2012).

[3] L. J. Miara, S. P. Ong, Y. Mo, W. D. Richards, Y. Park, J.-M. Lee, H. S. Lee, and G. Ceder, *Chem. Mater.* **25**, 3048 (2013).

[4] Y. Wang, W. D. Richards, S. P. Ong, L. J. Miara, J. C. Kim, Y. Mo, and G. Ceder, *Nat. Mater.* **14**, 1026 (2015).

[5] A. Hooper and B. C. Tofield, *J. Power Sources* **11**, 33 (1984).

[6] E. J. Cussen, *J. Mater. Chem.* **20**, 5167 (2010).

[7] V. Thangadurai and W. Weppner, Ionics **12**, 81 (2006).

[8] R. Murugan, V. Thangadurai, and W. Weppner, *Angew. Chem. Int. Ed.* **46**, 7778 (2007).

[9] Y. Li, J.-T. Han, C.-A. Wang, H. Xie, and J. B. Goodenough, *J. Mater. Chem.* **22**, 15357 (2012).

[10] H. Xie, K.-S. Park, J. Song, and J. B. Goodenough, *Electrochem. Commun.* **19**, 135 (2012).

[11] R. Satish, V. Aravindan, W. C. Ling, J. B. Goodenough, and S. Madhavi, *Adv. Energy Mater.* **4** (2014).

[12] S. Geller, *Z. Kristallogr. Cryst. Mater.* **125**, 1 (1967).

[13] S. Abrahams and S. Geller, *Acta Crystallog.* **11**, 437 (1958).

[14] Z. Deng, B. Radhakrishnan, and S. P. Ong, *Chem. Mater.* **27**, 3749 (2015).

[15] Z. Deng, Z. Wang, I.-H. Chu, J. Luo, and S. P. Ong, *J. Electrochem. Soc.* **163**, A67 (2016).

[16] I.-H. Chu, H. Nguyen, S. Hy, Y.-C. Lin, Z. Wang, Z. Xu, Z. Deng, Y. S. Meng, and S. P. Ong, *ACS Appl. Mater. Interfaces* **8**, 7843 (2016).

[17] Z. Deng, Z. Zhu, I.-H. Chu, and S. P. Ong, *Chem. Mater.* **29**, 281 (2017).

[18] Z. Zhu, I.-H. Chu, and S. P. Ong, *Chem. Mater.* **29**, 2474 (2017).

[19] Y. Zhu, X. He, and Y. Mo, *ACS Appl. Mater. Interfaces* **7**, 23685 (2015).

[20] F. Han, Y. Zhu, X. He, Y. Mo, and C. Wang, *Adv. Energy Mater.* **6**, 1501590 (2016).

[21] Y. Zhu, X. He, and Y. Mo, *J. Mater. Chem. A* **4**, 3253 (2016).

[22] X. He, Y. Zhu, and Y. Mo, *Nat. Commun.* **8**, 15893 (2017).

[23] S. Kirklin, B. Meredig, and C. Wolverton, *Adv. Energy Mater.* **3**, 252 (2013).

[24] M. Liu, Z. Rong, R. Malik, P. Canepa, A. Jain, G. Ceder, and K. A. Persson, *Energy Environ. Sci.* **8**, 964 (2015).

[25] A. Urban, I. Matts, A. Abdellahi, and G. Ceder, *Adv. Energy Mater.* **6**, 1600488 (2016).

[26] S. Kim, M. Aykol, V. I. Hegde, Z. Lu, S. Kirklin, J. R. Croy, M. M. Thackeray, and C. Wolverton, *Energy Environ. Sci.* **10**, 2201 (2017).

[27] M. Aykol, S. Kirklin, and C. Wolverton, *Adv. Energy Mater.* **4**, 1400690 (2014).

[28] M. Aykol, S. Kim, V. I. Hegde, D. Snydacker, Z. Lu, S. Hao, S. Kirklin, D. Morgan, and C. Wolverton, *Nat. Commun.* **7**, 13779 (2016).

[29] J. E. Saal, S. Kirklin, M. Aykol, B. Meredig, and C. Wolverton, *JOM* **65**, 1501 (2013).

[30] S. Kirklin, J. E. Saal, B. Meredig, A. Thompson, J. W. Doak, M. Aykol, S. Rühl, and C. Wolverton, *npj Comput. Mater.* **1**, 15010 (2015).

[31] G. Kresse and J. Hafner, *Phys. Rev. B* **47**, 558 (1993).

[32] G. Kresse and J. Furthmüller, Comput. Mater. Sci. **6**, 15 (1996).

[33] G. Kresse and J. Furthmüller, *Phys. Rev. B* **54**, 11169 (1996).

[34] M.W. Chase, J.R. Downey, D.J. Frurip, R.A. McDonald, and A.N. Syverud, *J. Phys. Chem. Ref. Data* **14** (1985).

[35] K. Momma, and F. Izumi, *J. Appl. Crystallogr.* **44**, 1272 (2011).

[36] R. D. Shannon, *Acta Crystallog. A* **32**, 751 (1976).

[37] See Supplemental Material at [URL will be inserted by publisher] for the list of Li_3-garnets studied, bulk lithiation voltage profiles and Arrhenius plots of Li diffusion.

[38] S. Ramakumar, C. Deviannapoorani, L. Dhivya, L. S. Shankar, and R. Murugan, *Prog. Mater. Sci.* **88**, 325 (2017).

[39] M. Aykol, V.I. Hegde, S. Suram, L. Hung, P. Herring, C. Wolverton and J. Hommelshøj, arXiv:1806.05772.

[40] M. Park, X. Zhang, M. Chung, G. B. Less, and A. M. Sastry, *J. Power Sources* **195**, 7904 (2010).

[41] W. Luo, Y. Gong, Y. Zhu, K. K. Fu, J. Dai, S. D. Lacey, C. Wang, B. Liu, X. Han, Y. Mo, E. D. Wachsman, and L. Hu, *J. Am. Chem. Soc.* **138**, 12258 (2016).